Layered Rare-Earth Gallium Antimonides *RE*$GaSb_2$ (*RE* = La−Nd, Sm)

Allison M. Mills and Arthur Mar*

Contribution from the Department of Chemistry, University of Alberta, Edmonton, AB, Canada T6G 2G2

Received October 17, 2000

Abstract: The ternary rare-earth gallium antimonides, *RE*$GaSb_2$ (*RE* = La−Nd, Sm), have been synthesized through reaction of the elements. The structures of $SmGaSb_2$ (orthorhombic, space group D_2^5-$C222_1$, $Z = 4$, $a = 4.3087(5)$ Å, $b = 22.093(4)$ Å, $c = 4.3319(4)$ Å) and $NdGaSb_2$ (tetragonal, space group D_{4h}^{19}-$I4_1/amd$, $Z = 8$, $a = 4.3486(3)$ Å, $c = 44.579(8)$ Å) have been determined by single-crystal X-ray diffraction. The $SmGaSb_2$-type structure is adopted for *RE* = La and Sm, whereas the $NdGaSb_2$-type structure is adopted for *RE* = Ce−Nd. The layered $SmGaSb_2$ and $NdGaSb_2$ structures are stacking variants of each other. In both structures, two-dimensional layers of composition $^2_\infty$[GaSb] are separated from square nets of Sb atoms $^2_\infty$[Sb] by *RE* atoms. Alternatively, the structures may be considered as resulting from the insertion of zigzag Ga chains between $^2_\infty$[*RE* Sb_2] slabs. In $SmGaSb_2$, all of the Ga chains are parallel and the $^2_\infty$[$SmSb_2$] layers are stacked in a $ZrSi_2$-type arrangement. In $NdGaSb_2$, the Ga chains alternate in direction, resulting in a doubling of the long axis relative to $SmGaSb_2$, and the $^2_\infty$[$NdSb_2$] layers are stacked in a $Zr_3Al_4Si_5$-type arrangement. Extended Hückel band structure calculations are used to explain the bonding in the $[GaSb_2]^{3-}$ substructure.

Introduction

A large number of alkali− and alkaline-earth−metal gallium antimonides with a remarkable variety of structures have been characterized.[1] The bonding in these compounds can be successfully rationalized by using the Zintl concept.[2] Accordingly, the more electropositive alkali or alkaline-earth metal donates its valence electrons to the more electronegative main group elements, which then form bonds, homoatomic ones if necessary, to satisfy the octet rule. The resulting anionic substructures are manifested as discrete $GaSb_3$ trigonal planar or $GaSb_4$ tetrahedral units, or extended networks built up from these units. All exhibit strong covalent bonds between atoms with completed valence shells, as is characteristic of normal valence compounds.

Reduced electronegativity differences between the electropositive and electronegative components render the applicability of the Zintl concept on more questionable grounds. As one moves leftward in the periodic table in choosing the electronegative (p-block) component, toward the group 13 and 14 elements, clusters and networks abound in the resulting structures.[2] But one can also move rightward in the periodic table in choosing the electropositive element, although such cases have not been examined as extensively. For many ternary rare-earth main-group-element antimonides, the occurrence of nonclassical bonding patterns requires that multicenter or partial bonding be invoked.[3] In our attempts to extend the diverse structural chemistry of the alkali− or alkaline-earth−metal gallium antimonides to rare-earth analogues, we have recently isolated the first examples of rare-earth gallium antimonides, $La_{13}Ga_8Sb_{21}$ and $RE_{12}Ga_4Sb_{23}$ (*RE* = La−Nd, Sm).[4] Both of these structures contain the characteristic trigonal planar $GaSb_3$ units of the alkali and alkaline-earth metal gallium antimonides, as well as more unusual Ga−Ga and Sb−Sb homoatomic bonding networks. One-dimensional square ribbons with intermediate Sb−Sb bonding are linked by either Ga_2-pairs (in $RE_{12}Ga_4Sb_{23}$) or six-membered Ga rings (in $La_{13}Ga_8Sb_{21}$). Here, we report the synthesis of a series of rare-earth gallium antimonides, *RE*$GaSb_2$ (*RE* = La−Nd, Sm), that crystallize in one of two structure types, $SmGaSb_2$ (for *RE* = La, Sm) or $NdGaSb_2$ (for *RE* = Ce−Nd). In the *RE*$GaSb_2$ structures, we find two-dimensional "Zintl layers" containing strong homoatomic Ga−Ga bonding in zigzag chains, in addition to strong Ga−Sb bonding. These alternate with Sb square sheets containing multicenter Sb−Sb bonding that are typical of binary and ternary rare-earth antimonides. The *RE*$GaSb_2$ compounds are the newest members of a growing family of rare-earth main-group antimonides, $REM_{1-x}Sb_2$ (M = In, Sn), featuring strong M−M and M−Sb bonding in $^2_\infty$[MSb] layers and intermediate Sb−Sb bonding in square nets.[5,6]

Experimental Section

Synthesis. Starting materials were powders of the rare-earth elements (99.9%, Alfa-Aesar), antimony powder (99.995%, Aldrich), and gallium granules (99.9999%, Alfa-Aesar). Reactions were carried out on a 0.4-g

* To whom correspondence should be addressed. Telephone: (780) 492-5592. Fax: (780) 492-8231. E-mail: arthur.mar@ualberta.ca.

(1) For example, see the following. (a) $Na_2Ga_3Sb_3$: Cordier, G.; Ochmann, H.; Schäfer, H. *Mater. Res. Bull.* **1986**, *21*, 331. (b) Sr_3GaSb_3: Cordier, G.; Schäfer, H.; Stelter, M. *Z. Naturforsch. B: Chem. Sci.* **1987**, *42*, 1268. (c) $K_{20}Ga_6Sb_{12.66}$: Cordier, G.; Ochmann, H. *Z. Naturforsch. B: Chem. Sci.* **1990**, *45*, 277. (d) Cs_6GaSb_3: Blase, W.; Cordier, G.; Somer, M. *Z. Kristallogr.* **1992**, *199*, 277. (e) $Na_3Sr_3GaSb_4$: Somer, M.; Carrillo-Cabrera, W.; Nuss, J.; Peters, K.; von Schnering, H. G.; Cordier, G. *Z. Kristallogr.* **1996**, *211*, 479. (f) Eisenmann, B.; Cordier, G. In *Chemistry, Structure, and Bonding of Zintl Phases and Ions*; Kauzlarich, S. M., Ed.; VCH Publishers: New York, 1996; p 61.

(2) (a) *Chemistry, Structure, and Bonding of Zintl Phases and Ions*; Kauzlarich, S. M., Ed.; VCH Publishers: New York, 1996. (b) Corbett, J. D. *Angew. Chem., Int. Ed. Engl.* **2000**, *39*, 670.

(3) Papoian, G. A.; Hoffmann, R. *Angew. Chem., Int. Ed. Engl.* **2000**, *39*, 2408.

(4) Mills, A. M.; Mar, A. *Inorg. Chem.* **2000**, *39*, 4599.

(5) Ferguson, M. J.; Ellenwood, R. E.; Mar, A. *Inorg. Chem.* **1999**, *38*, 4503.

(6) Ferguson, M. J.; Hushagen, R. W.; Mar, A. *Inorg. Chem.* **1996**, *35*, 4505.

10.1021/ja003705+ CCC: $20.00
Published on Web 01/23/2001

Table 1. Cell Parameters for Ternary *RE*$GaSb_2$ Compounds

compound	structure type	*a* (Å)	*b* (Å)	*c* (Å)	*V* (Å^3)
$LaGaSb_2$	$SmGaSb_2$-type	4.382(3)	22.775(13)	4.474(3)	446.5(4)
$CeGaSb_2$	$NdGaSb_2$-type	4.3708(16)	4.3708(16)	45.07(2)	860.9(6)
$PrGaSb_2$	$NdGaSb_2$-type	4.3599(16)	4.3599(16)	44.81(2)	851.8(5)
$NdGaSb_2$	$NdGaSb_2$-type	4.3427(15)	4.3427(15)	44.545(19)	840.1(5)
$SmGaSb_2$	$SmGaSb_2$-type	4.304(3)	22.121(13)	4.320(3)	411.3(3)

scale in evacuated fused-silica tubes (8-cm length; 10-mm i.d.). Elemental compositions were determined by EDX (energy-dispersive X-ray) analysis on a Hitachi S-2700 scanning electron microscope. X-ray powder patterns were collected on an Enraf-Nonius FR552 Guinier camera (Cu Kα_1 radiation; Si standard) and analyzed with the Filmscan and Jade 3.0 software packages.[7]

Attempts to grow single crystals of $La_{13}Ga_8Sb_{21}$ with use of a tin flux led to isolation of a new series of compounds of composition $LaGa_{1-x}Sn_xSb_2$. The Sn-rich end member of this series, $LaSn_{0.75}Sb_2$, has been described previously.[6] Although this reaction method yields large single crystals, some Sn is always incorporated into the product, and we were unable to synthesize the Ga-rich end member $LaGaSb_2$ by this route. Subsequent stoichiometric reactions at the composition *RE*$GaSb_2$ (*RE* = La−Nd, Sm) led to the formation of products that were significantly contaminated with the $Pr_{12}Ga_4Sb_{23}$-type phases, except in the case of Sm. Single black platelike crystals of $SmGaSb_2$ (Anal. (mol %): Sm 28.4(5), Ga 21.1(2), Sb 50.4(5) (average of 4 analyses)) were obtained from a reaction of Sm, Ga, and Sb in the ratio 1:1:2 heated at 900 °C for 3 days, cooled to 500 °C over 4 days, then cooled to 20 °C over 18 h. Use of an excess of Ga minimizes the formation of $Pr_{12}Ga_4Sb_{23}$-type impurities. Mixtures of the elements *RE* (*RE* = La−Nd), Ga, and Sb in the ratio 1:2:2, heated as before, resulted in powder products of *RE*$GaSb_2$ that invariably contained unreacted Ga. The powder patterns of these products indicated that only $LaGaSb_2$ crystallizes in the orthorhombic $SmGaSb_2$-type phase. A more symmetric tetragonal phase is adopted by *RE* = Ce−Nd. Gray rectangular plates of $NdGaSb_2$ (Anal. (mol %): Nd 24.8(3), Ga 27(1), Sb 48(1) (average of 2 analyses)) were isolated from a reaction of Nd, Ga, and Sb in the ratio 1:2:2 heated at 800 °C for 3 days and then cooled to 20 °C over 18 h. The powder patterns of the *RE*$GaSb_2$ phases, prepared at 900 °C as described above, were indexed, and the cell parameters refined with the use of the program POLSQ[8] are given in Table 1.

Structure Determination. Preliminary cell parameters for $SmGaSb_2$ and $NdGaSb_2$ were determined from Weissenberg photographs. Final cell parameters were determined from least-squares analysis of the setting angles of 24 reflections centered on an Enraf-Nonius CAD4 diffractometer in the range $20° \le 2\theta$ (Mo Kα) $\le 50°$ for $SmGaSb_2$ and $20° \le 2\theta$ (Mo *K*α) $\le 42°$ for $NdGaSb_2$. Intensity data were collected at 22 °C with the $\theta-2\theta$ scan technique in the range $4° \le 2\theta$(Mo Kα) $\le 70°$. Crystal data and further details of the data collections are given in Table 2. All calculations were carried out using the SHELXTL (Version 5.1) package.[9] Conventional atomic scattering factors and anomalous dispersion corrections were used.[10] Intensity data were reduced and averaged, and face-indexed numerical absorption corrections were applied in XPREP. Initial atomic positions were located by direct methods with XS, and refinements were performed by least-squares methods with XL.

Weissenberg photographs of $SmGaSb_2$ displayed Laue symmetry *mmm* and systematic extinctions (*hkl*, $h + k = 2n + 1$; 00*l*, $l = 2n + 1$) consistent uniquely with the noncentrosymmetric orthorhombic space group $C222_1$. In particular, inspection of the *h*0*l* reflections with $l = 2n + 1$ in the reciprocal space plots clearly confirmed the absence of a *c*-glide plane in $SmGaSb_2$ (out of 38 such data, 17 had $I > 3\sigma(I)$), ruling out the centrosymmetric space group *Cmcm*. The initial positions of the *RE* and Sb atoms in $SmGaSb_2$ ($C222_1$) were taken from those in the closely related structure of $LaSn_{0.75}Sb_2$ (*Cmcm*).[6] A first refinement revealed considerable electron density at a site located between [$SmSb_2$] layers. This site was assigned to Ga based on reasonable Ga−Sb(1) and Ga−Ga distances. The Ga atoms form chains running along the *c*-axis that impart chirality to the $SmGaSb_2$ structure. In accordance with the calculated Flack parameter of 0.54(6),[11] the structure was refined as a racemic twin. Since substoichiometric occupation of the Sn site was observed in $LaSn_{0.75}Sb_2$, refinements were performed in which the occupancies of successive atoms were allowed to vary. These resulted in essentially 100% occupancy for all atoms, including Ga, giving the formula $SmGaSb_2$, consistent with the EDX analyses.

Table 2. Crystallographic Data for $SmGaSb_2$ and $NdGaSb_2$

formula	$SmGaSb_2$	$NdGaSb_2$
formula mass (amu)	463.57	457.46
space group	D_2^5-$C222_1$ (No. 20)	D_{4h}^{19}-$I4_1/amd$ (No. 141)
a (Å)[a]	4.3087(5)	4.3486(3)
b (Å)[a]	22.093(4)	4.3486(3)
c (Å)[a]	4.3319(4)	44.579(8)
V (Å^3)	412.36(10)	843.0(2)
Z	4	8
T (°C)	22	22
λ (Å)	0.710 73	0.710 73
ρ_{calcd} (g cm^{-3})	7.467	7.209
μ(Mo Kα) (cm^{-1})	332.1	308.8
$R(F)$ for $F_o^2 > 2\sigma(F_o^2)$[b]	0.029	0.034
$R_w(F_o^2)$[c]	0.074	0.073

[a] Obtained from a refinement constrained so that $\alpha = \beta = \gamma = 90°$, and additionally for $NdGaSb_2$, $a = b$. [b] $R(F) = \sum||F_o| - |F_c||/\sum|F_o|$. [c] $R_w(F_o^2) = [\sum[w(F_o^2 - F_c^2)^2]/\sum wF_o^4]^{1/2}$; $w^{-1} = [\sigma^2(F_o^2) + (ap)^2 + bp]$ where $p = [\max(F_o^2,0) + 2F_c^2]/3$. For $SmGaSb_2$, $a = 0.0308$, $b = 7.8140$; for $NdGaSb_2$, $a = 0.0229$, $b = 30.9047$.

Reciprocal space plots of $NdGaSb_2$ revealed tetragonal Laue symmetry 4/*mmm* and systematic extinctions (*hkl*, $h + k + l = 2n + 1$; *hk*0, $h = 2n + 1$; *hhl*, $2h + l = 4n + 1$, 2, or 3) consistent uniquely with the space group $I4_1/amd$. Initial positions for the Nd and Sb atoms were found by direct methods. An initial refinement revealed additional electron density between [$NdSb_2$] layers that was assigned as Ga by analogy with $SmGaSb_2$. In this case, however, the mirror plane at (0 *y z*) generates two sets of Ga zigzag chains, resulting in close Ga−Ga contacts (1.43 and 2.17 Å). The Ga site must, therefore, have a maximum occupancy of 50% (only one set of Ga chains may be present). The possibility that the disorder in the Ga position is a consequence of improper choice of space group was considered; however, the disordered Ga chains reappeared when the structure was solved in the noncentrosymmetric orthorhombic space group $I2_12_12_1$. As above, refinements allowing the occupancies of successive atoms to vary freely resulted in essentially half occupancy for the Ga site and full occupancy for all other atoms. The final formula, $NdGaSb_2$ (with $Z = 8$), is consistent with EDX analyses.

In both cases, the final refinement led to a featureless electron density map ($\Delta\rho_{max} = 3.32$, $\Delta\rho_{min} = -3.52$ e Å^{-3} for $SmGaSb_2$; $\Delta\rho_{max} = 3.22$, $\Delta\rho_{min} = -1.95$ e Å^{-3} for $NdGaSb_2$) and to reasonable displacement parameters for all atoms, except Ga. The components of the Ga thermal ellipsoids in the plane of the Ga chains are somewhat large in both structures. This behavior may represent the tendency of the atoms inserted between the [*RE*Sb_2] layers to disorder over several sites, as has been observed in $LaSn_{0.75}Sb_2$.[6] The atomic positions of $SmGaSb_2$ and $NdGaSb_2$ were standardized with the program STRUCTURE TIDY.[12] Final values of the positional and displacement parameters are given in Table 3. Interatomic distances are listed in Table 4. Powder diffraction data, additional crystal data, anisotropic displacement parameters, bond angles, and CIFs are available as Supporting Information, and structure amplitudes are available from the authors.

Band Structure. A tight-binding extended Hückel band structure calculation was performed on the anionic $[GaSb_2]^{3-}$ substructure of $SmGaSb_2$ with use of the EHMACC suite of programs.[13,14] The atomic

(7) *Filmscan* and *Jade 3.0*; Materials Data Inc.: Livermore, CA, 1996.
(8) POLSQ: Program for least-squares unit cell refinement. Modified by D. Cahen and D. Keszler, Northwestern University, 1983.
(9) Sheldrick, G. M. *SHELXTL* Version 5.1; Bruker Analytical X-ray Systems, Inc.: Madison, WI, 1997.
(10) *International Tables for X-ray Crystallography*; Wilson, A. J. C., Ed.; Kluwer: Dordrecht, The Netherlands, 1992; Vol. C.
(11) Flack, H. D. *Acta Crystallogr., Sect. A: Found. Crystallogr.* **1983**, *39*, 876.
(12) Gelato, L. M.; Parthé, E. *J. Appl. Crystallogr.* **1987**, *20*, 139.
(13) Whangbo, M.-H.; Hoffmann, R. *J. Am. Chem. Soc.* **1978**, *100*, 6093.

Table 3. Positional and Equivalent Isotropic Displacement Parameters for $SmGaSb_2$ and $NdGaSb_2$

atom	Wyckoff position	*x*	*y*	*z*	U_{eq} (Å^2)[a]
			$SmGaSb_2$		
Sm	4*b*	0	0.138632(18)	1/4	0.00760(12)
Ga	4*a*	0.1538(4)	0	0	0.0232(3)
Sb(1)	4*b*	0	0.40698(3)	1/4	0.00881(13)
Sb(2)	4*b*	0	0.75016(2)	1/4	0.00795(13)
			$NdGaSb_2$		
Nd	8*e*	0	1/4	0.069357(14)	0.00908(16)
Ga[b]	16*f*	0.1649(7)	0	0	0.0345(7)
Sb(1)	8*e*	0	1/4	0.203764(18)	0.01077(18)
Sb(2)	4*b*	0	1/4	3/8	0.0100(2)
Sb(3)	4*a*	0	3/4	1/8	0.0096(2)

[a] U_{eq} is defined as one-third of the trace of the orthogonalized U_{ij} tensor. [b] Occupancy of 0.50.

Table 4. Selected Interatomic Distances (Å) in $SmGaSb_2$ and $NdGaSb_2$

$SmGaSb_2$		$NdGaSb_2$	
Sm−Sb(1)	3.2169(3) (×4)	Nd−Sb(1)	3.2431(4) (×4)
Sm−Sb(2)	3.2730(6) (×2)	Nd−Sb(2)	3.2986(6) (×2)
Sm−Sb(2)	3.2754(6) (×2)	Nd−Sb(3)	3.2986(6) (×2)
Sm−Ga	3.3155(7) (×2)	Nd−Ga	3.3549(10) (×2)
Ga−Ga	2.539(2) (×2)	Ga−Ga	2.605(3) (×2)
Ga−Sb(1)	2.7606(12) (×2)	Ga−Sb(1)	2.7485(17) (×2)
Sb(2)−Sb(2)	3.0549(2) (×4)	Sb(2)−Sb(3)	3.0749(2) (×4)

Table 5. Extended Hückel Parameters

atom	orbital	H_{ii} (eV)	ζ_{i1}
Ga	4s	−14.58	1.77
	4p	−6.75	1.55
Sb	5s	−18.8	2.323
	5p	−11.7	1.999

parameters used are listed in Table 5.[15,16] Properties were extracted from the band structure using 108 *k* points in the irreducible portion of the Brillouin zone.

Results and Discussion

Structures. The structures of $SmGaSb_2$ (Figure 1) and $NdGaSb_2$ (Figure 2) are closely related. Both are composed of two-dimensional anionic layers of composition $^2_\infty$[GaSb] and $^2_\infty$[Sb] separated by *RE* atoms. Different stacking arrangements of these layers generate the two structure types. We will first describe the features common to both structure types, and then consider the relationship between them.

The $^2_\infty$[GaSb] layers are "Zintl layers" containing strong covalent bonding. Each Ga atom is coordinated by two Sb(1) atoms and two other Ga atoms ($SmGaSb_2$, Ga−Sb(1) 2.7606(12) Å, Ga−Ga 2.539(2) Å; $NdGaSb_2$, Ga−Sb(1) 2.7485(17) Å, Ga−Ga 2.605(3) Å) in a distorted tetrahedral fashion (Figure 3a). The Ga atoms that are viewed as the ligands in a given $Ga(Ga_2Sb_2)$ tetrahedron serve as centers of adjacent coordination polyhedra so as to form infinite one-dimensional zigzag Ga chains. Parallel Ga chains are then joined by Ga−Sb bonding to complete the $^2_\infty$[GaSb] layer. In the case of $NdGaSb_2$, the zigzag Ga chains are disordered over two possible configurations, as shown in Figure 4. Ga-centered tetrahedra are the basic building blocks of many alkali- and alkaline-earth-metal gallium antimonide Zintl phases, and the Ga−Sb bond distances in these phases are similar to those above (for example, the chains of

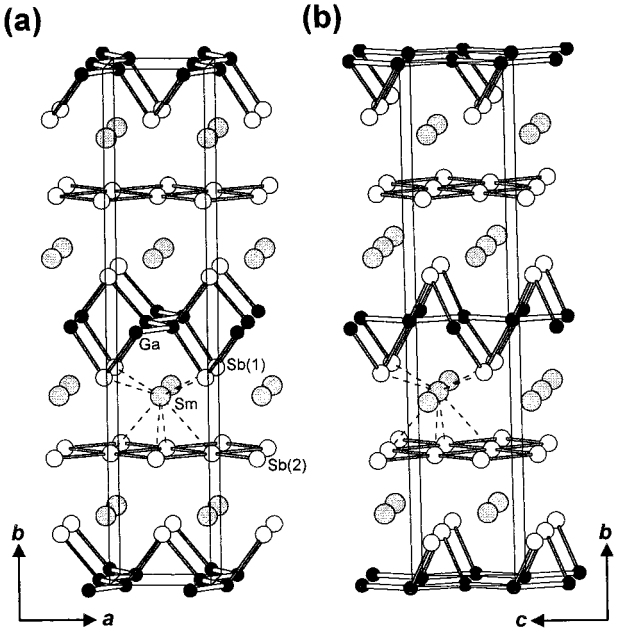

Figure 1. Views of $SmGaSb_2$ (a) down the *c* axis and (b) down the *a* axis showing the unit cell outline and the labeling scheme. The large lightly shaded circles are Sm atoms, the small solid circles are Ga atoms, and the medium open circles are Sb atoms.

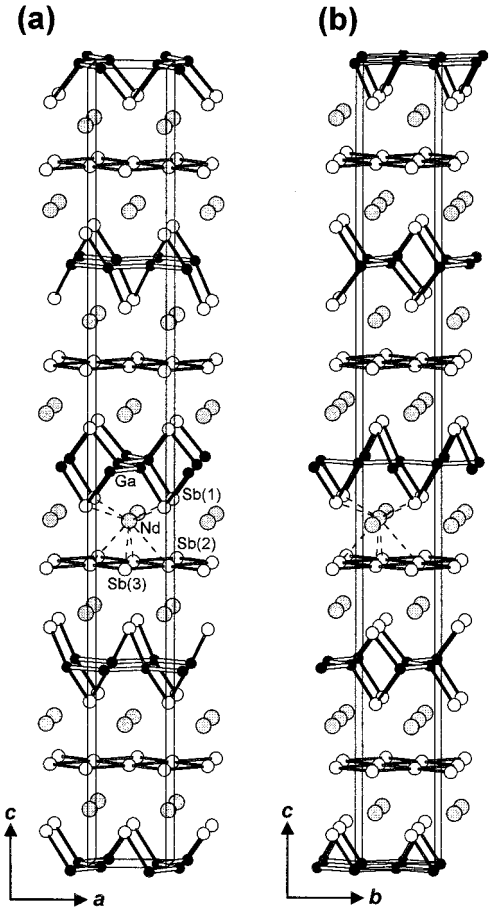

Figure 2. Views of $NdGaSb_2$ (a) down the *b* axis and (b) down the *a* axis showing the unit cell outline and the labeling scheme. The large lightly shaded circles are Nd atoms, the small solid circles are Ga atoms, and the medium open circles are Sb atoms.

(14) Hoffmann, R. *Solids and Surfaces: A Chemist's View of Bonding in Extended Structures*; VCH Publishers: New York, 1988.
(15) Canadell, E.; Eisenstein, O.; Rubio, J. *Organometallics* **1984**, *3*, 759.
(16) Hughbanks, T.; Hoffmann, R.; Whangbo, M.-H.; Stewart, K. R.; Eisenstein, O.; Canadell, E. *J. Am. Chem. Soc.* **1982**, *104*, 3876.

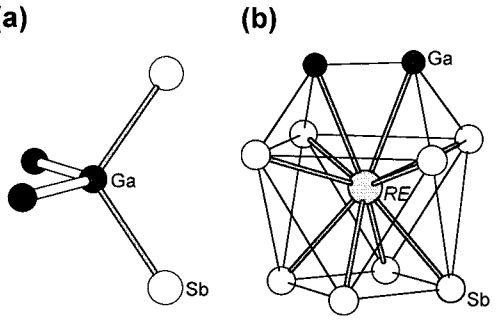

Figure 3. (a) Distorted tetrahedral coordination around Ga in $SmGaSb_2$ and $NdGaSb_2$. (b) Coordination environment around *RE* atoms in $SmGaSb_2$ and $NdGaSb_2$.

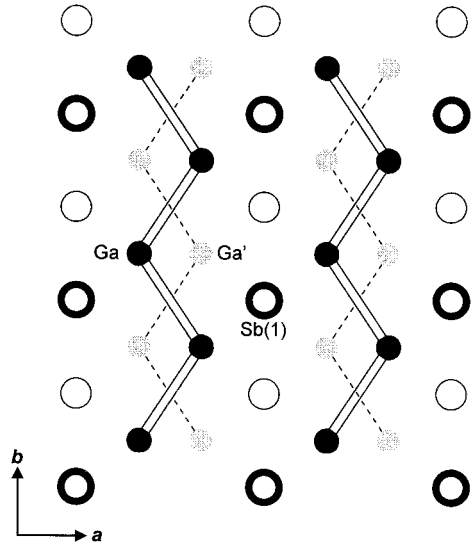

Figure 4. View down the *c* axis of a $^2_\infty$[GaSb] layer in $NdGaSb_2$ showing the disorder of the zigzag Ga chains, associated with a 50% occupancy of the Ga site. Sb atoms with thick rims reside on planes displaced perpendicular to the plane of the page relative to those with thin rims.

corner-sharing $GaSb_4$ tetrahedra in Sr_3GaSb_3 contain Ga−Sb distances of 2.642−2.798 Å[2b]). The $^2_\infty$[GaSb] layer contains Ga−Ga bonding, which, while unusual for alkali- and alkaline-earth−metal gallium antimonides, appears to be a recurring feature in rare-earth−metal gallium antimonides. Only one antimonide Zintl phase, $Na_2Ga_3Sb_3$, features a Ga−Ga bond (2.541(3) Å).[2a] However, the zigzag Ga chains in $SmGaSb_2$ and $NdGaSb_2$ resemble, but differ in conformation from, the cis−trans Ge chains formed by a similar connectivity of $Ge(Ge_2As_2)$ tetrahedra found in the three-dimensional anionic substructure of $BaGe_2As_2$.[17] Isolated Ga zigzag chains with Ga−Ga bond distances (2.623(1) Å) comparable to those in $SmGaSb_2$ and $NdGaSb_2$ are contained in the binary gallide Li_2Ga.[18]

Within the $^2_\infty$[Sb] layers of $SmGaSb_2$ and $NdGaSb_2$, each Sb atom is bonded to four other Sb atoms ($SmGaSb_2$, Sb(2)−Sb(2) 3.0549(2) Å; $NdGaSb_2$, Sb(2)−Sb(3) 3.0749(2) Å), forming a flat square sheet. (Even though $SmGaSb_2$ is orthorhombic, the Sb(2)−Sb(2)−Sb(2) angles are close to 90° (89.692(9)−90.307(9)°) as a result of the *a* and *c* parameters being nearly the same.) These Sb−Sb distances are long compared to the intralayer Sb−Sb bond length (2.908 Å) but shorter than the weakly bonding interlayer distance (3.355 Å) in elemental Sb.[19] Rather, they are typical of the Sb−Sb distances occurring in the Sb square sheets of $SmSb_2$ (3.03(2)−3.09(2) Å)[20] or $REM_{1-x}Sb_2$ (3.097(2) Å for M = Zn;[21] 3.119(3)−3.142(3) Å for M = In;[5] 3.0952(3) Å for M = Sn[6]). In these binary and ternary rare-earth antimonides, extension of the Zintl concept to account for partial bond order leads to the interpretation of such intermediate Sb−Sb bonds as one-electron or half-bonds, to a first approximation.[3,5,6]

The *RE* atoms, located between the $^2_\infty$[GaSb] and $^2_\infty$[Sb] layers, center square antiprism-based polyhedra, as is typical in structures containing Sb square sheets and ribbons (Figure 3b).[4−6,20,21] Each *RE* atom is coordinated by eight Sb atoms: four Sb(1) atoms from the $^2_\infty$[GaSb] layer define one square face, and four Sb(2) (in $SmGaSb_2$), or two Sb(2) and two Sb(3) (in $NdGaSb_2$), atoms from the $^2_\infty$[Sb] net define the second square face ($SmGaSb_2$, Sm−Sb 3.2169(3)−3.2754(6) Å; $NdGaSb_2$, Nd−Sb 3.2431(4)−3.2986(6) Å). Two Ga atoms then cap the larger Sb(1) square face ($SmGaSb_2$, Sm−Ga 3.3155(7) Å; $NdGaSb_2$, Nd−Ga 3.3549(10) Å). Similar Ga-capped Sb antiprisms surrounding *RE* atoms are found in $La_{13}Ga_8Sb_{21}$ and $RE_{12}Ga_4Sb_{23}$. The *RE*−Sb and *RE*−Ga distances in $Sm_{12}Ga_4Sb_{23}$ (Sm−Sb 3.174(2)−3.304(2), Sm−Ga 3.232(2)−3.353(2) Å) or $Nd_{12}Ga_4Sb_{23}$ (Nd−Sb 3.211(1)−3.341(1), Nd−Ga 3.270(1)−3.393(1) Å) are comparable to those above.[22]

The portrayal of the $SmGaSb_2$ and $NdGaSb_2$ structures in Figures 1 and 2, respectively, emphasizes the covalent layered networks $^2_\infty$[GaSb] and $^2_\infty$[Sb] between which *RE* atoms are inserted. But it is equally valid to consider the structures as stacked slabs of composition $^2_\infty[RESb_2]$ between which zigzag Ga chains are to be inserted. Within such $^2_\infty[RESb_2]$ slabs, the *RE* atoms are positioned above and below the $^2_\infty$[Sb] square sheet such that no two *RE* atoms share the same square face. Sandwiching these are the Sb(1) atoms arranged in nearly square ($SmGaSb_2$) or square ($NdGaSb_2$) nets that are half as dense as the $^2_\infty$[Sb] sheet and whose dimensions are defined by the cell parameters in the plane of the nets. The stacking of the $^2_\infty[RESb_2]$ slabs determines the orientation in which the inserted zigzag Ga chains run, since each Ga atom must be bonded to two Sb(1) atoms, one in the $^2_\infty[RESb]_2$ slab above and one below it. As shown in Figures 1 and 2, all of the zigzag Ga chains in $SmGaSb_2$ are parallel and run along the *c*-direction, whereas the zigzag Ga chains in $NdGaSb_2$ are mutually perpendicular and alternately run along the *a*- or *b*-direction. In $SmGaSb_2$, the $^2_\infty[RESb_2]$ slabs are mutually displaced by $^1/_2\vec{a}$ as they are stacked along the *b*-axis, so that two such slabs are needed before the sequence is repeated. In $NdGaSb_2$, the $^2_\infty[RESb_2]$ slabs are mutually displaced alternately by $^1/_2\vec{a}$ *and* $^1/_2\vec{b}$ as they are stacked along the *c*-axis, so that four such slabs are needed before the sequence is repeated. This difference in the stacking sequence of the $^2_\infty[RESb_2]$ slabs causes the stacking axis (*c*) in $NdGaSb_2$ to be doubled with respect to the stacking axis (*b*) in $SmGaSb_2$.

Structural Relationships. This viewpoint of describing the stacking sequence of $^2_\infty[RESb_2]$ slabs followed by insertion of "guest" atoms is helpful in illuminating the structural relation-

(17) Eisenmann, B.; Schäfer, H. *Z. Naturforsch. B: Anorg. Chem. Org. Chem.* **1981**, *36*, 415.

(18) Müller, W.; Stöhr, J. *Z. Naturforsch. B: Anorg. Chem. Org. Chem.* **1977**, *32*, 631.

(19) Donohue, J. *The Structures of the Elements*; Wiley: New York, 1974.

(20) Wang, R.; Steinfink, H. *Inorg. Chem.* **1967**, *6*, 1685.

(21) Cordier, G.; Schäfer, H.; Woll, P. *Z. Naturforsch. B: Anorg. Chem. Org. Chem.* **1985**, *40*, 1097.

(22) The *RE*−Sb and *RE*−Ga bond lengths in $Sm_{12}Ga_4Sb_{23}$ and $Nd_{12}Ga_4Sb_{23}$ were calculated based on positional parameters from the crystal structure of $Pr_{12}Ga_4Sb_{23}$ and refined cell parameters from the powder patterns of $Sm_{12}Ga_4Sb_{23}$ and $Nd_{12}Ga_4Sb_{23}$, respectively.[4]

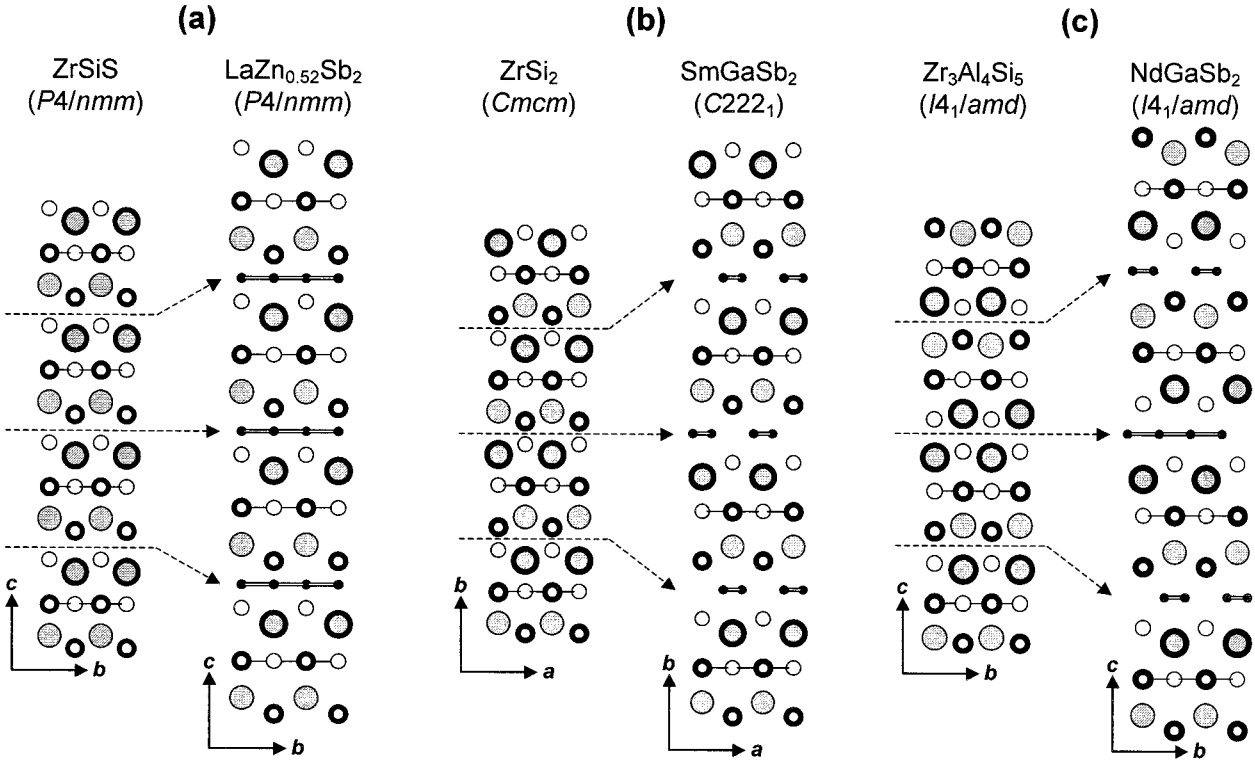

Figure 5. Comparison of the stacking sequence of $^2_\infty[RESb_2]$ slabs in ternary rare-earth antimonides $REM_{1-x}Sb_2$ and their relationship to simpler host structures in which *M* atoms are inserted. (a) AAAA stacking sequence (10 Å repeat) of slabs in ZrSiS-type and $LaZn_{0.52}Sb_2$ structures. (b) ABAB stacking sequence (20 Å repeat) of slabs in $ZrSi_2$-type and $SmGaSb_2$ structures. (c) ABCD stacking sequence (40 Å repeat) of slabs in $Zr_3Al_4Si_5$-type and $NdGaSb_2$ structures. The large lightly shaded circles are the electropositive atoms (Zr, Al, *RE*), the small solid circles are the *M* atoms (Zn, Ga), and the medium open circles are the other atoms *X* (Al, Si, Sb, S). Atoms with thick rims reside on planes displaced by half a unit cell parameter perpendicular to the plane of the page relative to those with thin rims. The inserted *M* atoms lie between these planes.

ships not only between $SmGaSb_2$ and $NdGaSb_2$ but also with many other structures. Indeed, $SmGaSb_2$ and $NdGaSb_2$ can be considered as stacking variants of ternary rare-earth antimonides $REM_{1-x}Sb_2$ with structures consisting of $^2_\infty[RESb_2]$ slabs separated by layers of *M* atoms. As shown in Figure 5, these ternary antimonides can also be derived from a simpler "host" structure.

Many binary rare-earth compounds REX_2 (X = S, Se, Te; P, As, Sb; Si, Ge) adopt the ZrSiS-type structure (Figure 5a) or distortions thereof, in which the nonmetal *X* occupies the Si and S sites.[23,24] In this structure, $^2_\infty[Zr(SiS)]$ slabs are stacked directly on top of each other along *c* without any displacement along *a* or *b*, and are held together by S−S bonds. This stacking arrangement generates a tetrahedral site that is occupied by Zn atoms in the structure of $LaZn_{0.52}Sb_2$, which consists of $^2_\infty[LaSb_2]$ slabs stacked in the same way as the $^2_\infty[Zr(SiS)]$ slabs in ZrSiS.[21] $LaZn_{0.52}Sb_2$ belongs to a large family of ternary rare-earth antimonides $REM_{1-x}Sb_2$ where the inserted *M* atoms can be not only Zn, but also many other transition or post-transition metals (M = Mn−Cu, Pd−Cd, Au).[21,25] This filled structure is known, among other labels, as the $HfCuSi_2$-type.[26] The binary rare-earth antimonide $YbSb_2$, containing divalent Yb, adopts the $ZrSi_2$-type structure (Figure 5b).[27,28] The $^2_\infty[ZrSi_2]$ slabs, which are held by Si−Si bonds, are displaced by $^1/_2\vec{a}$ as they are stacked along *b*, exactly in the same sequence as the $^2_\infty[SmSb_2]$ slabs in $SmGaSb_2$. A reduction in symmetry occurs as the Ga chains are inserted into the $ZrSi_2$-type structure (*Cmcm*) to form the $SmGaSb_2$ structure ($C222_1$). Finally, $NdGaSb_2$ represents a new stacking variant whose arrangement of $^2_\infty[NdSb_2]$ slabs has no counterpart in a simpler binary rare-earth structure, but does occur in the $^2_\infty[(Zr_{0.75}Al_{0.25})(Al_{0.38}Si_{0.62})_2]$ slabs found in the $Zr_3Al_4Si_5$-type structure (Figure 5c).[29] Insertion of the Ga chains into the $Zr_3Al_4Si_5$-type structure to form the $NdGaSb_2$ structure does not alter the space group ($I4_1/amd$) in this case because of the occurrence of disorder in the Ga chains (vide supra). With each $^2_\infty[RESb_2]$ slab being approximately 10 Å thick, the length of the stacking axis reflects the stacking sequence repeat for $LaZn_{0.52}Sb_2$ (∼10 Å), $SmGaSb_2$ (∼20 Å), and $NdGaSb_2$ (∼40 Å).

Comparison of $REGaSb_2$ to other representative members ($LaZn_{0.52}Sb_2$, $LaIn_{0.8}Sb_2$, and $LaSn_{0.75}Sb_2$) of this emerging class of ternary rare-earth antimonides $REM_{1-x}Sb_2$ illustrates the influence of valence electron count and size of the inserted *M* atoms on the structure adopted. As shown in Figure 6, the nature of the inserted *M* atoms determines not only the extent of possible *M*−*M* bonding, but also the directionality and strength

(23) Böttcher, P.; Doert, Th.; Arnold, H.; Tamazyan, R. *Z. Kristallogr.* **2000**, *215*, 246.
(24) Klein Haneveld, A. J.; Jellinek, F. *Recl. Trav. Chim. Pays-Bas* **1964**, *83*, 776.
(25) (a) Leithe-Jasper, A.; Rogl, P. *J. Alloys Compd.* **1994**, *203*, 133. (b) Sologub, O.; Hiebl, K.; Rogl, P.; Noël, H.; Bodak, O. *J. Alloys Compd.* **1994**, *210*, 153. (c) Sologub, O.; Noël, H.; Leithe-Jasper, A.; Rogl, P.; Bodak, O. I. *J. Solid State Chem.* **1995**, *115*, 441. (d) Sologub, O.; Hiebl, K.; Rogl, P.; Bodak, O. *J. Alloys Compd.* **1995**, *227*, 40. (e) Brylak, M.; Möller, M. H.; Jeitschko, W. *J. Solid State Chem.* **1995**, *115*, 305. (f) Wollesen, P.; Jeitschko, W.; Brylak, M.; Dietrich, L. *J. Alloys Compd.* **1996**, *245*, L5.
(26) Andrukhiv, L. S.; Lysenko, L. O.; Yarmolyuk, Ya. P.; Hladyshevsky, E. I. *Dopov. Akad. Nauk Ukr. RSR, Ser. A: Fiz.-Mat. Tekh. Nauki* **1975**, 645.
(27) Wang, R.; Bodnar, R.; Steinfink, H. *Inorg. Chem.* **1966**, *5*, 1468.
(28) Cotter, P. G.; Kohn, J. A.; Potter, R. A. *J. Am. Ceram. Soc.* **1956**, *39*, 11.
(29) Schubert, K.; Frank, K.; Gohle, R.; Maldonado, A.; Meissner, H. G.; Raman, A.; Rossteutscher, W. *Naturwissenschaften* **1963**, *50*, 41.

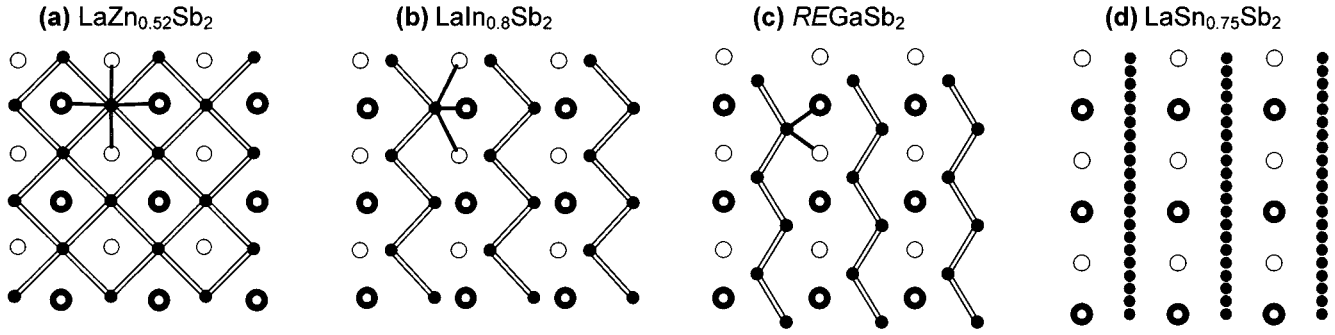

Figure 6. Comparison of the $^2_\infty$[*M*Sb] layers in (a) $LaZn_{0.52}Sb_2$, (b) $LaIn_{0.8}Sb_2$, (c) *RE*$GaSb_2$, and (d) $LaSn_{0.75}Sb_2$ shown in projection down the stacking direction. The small solid circles are the *M* atoms (Zn, In, Ga, Sn) and the open circles are the Sb atoms. Sb atoms with thick rims reside on planes displaced perpendicular to the plane of the page relative to those with thin rims. The inserted *M* atoms lie between these planes. The ideal square Zn net in $LaZn_{0.52}Sb_2$ is distorted to form zigzag Ga or In chains in $LaIn_{0.8}Sb_2$ and *RE*$GaSb_2$, and disordered linear Sn chains in $LaSn_{0.75}Sb_2$. Note also the shifting of the plane of Sb atoms with thick rims as this distortion occurs.

of *M*−Sb bonding, and hence ultimately the stacking arrangement. In $LaZn_{0.52}Sb_2$ (Figure 6a), the inserted Zn atoms form a perfectly square *M* net containing possibly weak Zn−Zn bonding.[21] (While d^{10}−d^{10} interactions may be questionable for Zn, they may be more plausible for Cd in the isostructural $LaCd_{0.7}Sb_2$.[25d,30]) The preference of Zn for a tetrahedral coordination dictates that the $^2_\infty$[$LaSb_2$] slabs be stacked directly on top of each other. Replacement of Zn by a more electron-rich main-group element such as Ga, In, or Sn is accompanied by distortion of the perfectly square *M* net to form main-group-element chains. In $LaIn_{0.8}Sb_2$ (Figure 6b), the square *M* net distorts to form parallel zigzag chains containing strong In−In bonding.[5] Each In atom is coordinated by three Sb atoms and two other In atoms in a distorted square pyramidal fashion. In *RE*$GaSb_2$ (Figure 6c), the distortion of the square *M* net is so severe that this description is no longer useful and the transition to *M* chains is fairly progressed. Each Ga atom is now coordinated by only two Sb atoms and two other Ga atoms in a tetrahedral fashion. Also consistent with the smaller size of Ga vs In, the Ga−Ga zigzag chains (∼2.5 Å) are coplanar, whereas the In−In zigzag chains (∼3.0 Å) are slightly canted with respect to the planes of the surrounding Sb sheets. Finally, in $LaSn_{0.75}Sb_2$, the even more electron-rich Sn atoms are inserted into partially occupied sites closely spaced in a nearly linear arrangement.[6] On a local level, a plausible interpretation is that each Sn atom is bonded strongly to two surrounding Sb atoms, or weakly to four Sb atoms, or somewhere between, depending on the site occupied.

The formation of parallel chains in $LaIn_{0.8}Sb_2$, *RE*$GaSb_2$, and $LaSn_{0.75}Sb_2$ requires a shifting of the Sb atoms above and below the *M* nets. To fulfill the *M*−Sb bonding requirements consistent with the preferred local coordination of *M*, adjacent $^2_\infty$[*RE*Sb_2] slabs must be displaced by half a unit cell length perpendicular to the chain direction (cf. Figure 6, part a vs parts b−d.) The stacking sequence of the $^2_\infty$[*RE*Sb_2] layers is identical in orthorhombic $SmGaSb_2$ and $LaSn_{0.75}Sb_2$ (Figure 5b) (and these compounds would be isostructural were it not for the different arrangement of the inserted *M* atoms). In monoclinic $LaIn_{0.8}Sb_2$, the adjacent slabs are shifted by slightly less than half a unit cell length with respect to one another, but the stacking arrangement is otherwise similar. Another consequence of the chain formation is to render inequivalent the lattice parameters in the plane of the *M* layers (with the exception of $NdGaSb_2$) as the symmetry is reduced from tetragonal ($LaZn_{0.52}Sb_2$) to orthorhombic ($SmGaSb_2$, $LaSn_{0.75}Sb_2$) to monoclinic ($LaIn_{0.8}Sb_2$). In $LaIn_{0.8}Sb_2$ (a = 4.521(3) Å, b = 4.331(3) Å) and $LaSn_{0.75}Sb_2$ (a = 4.2435(5) Å, c = 4.5053(6) Å), the difference between these parameters is relatively large. In these structures, there is only one energetically favorable way of placing the *M* chains over the $^2_\infty$[$LaSb_2$] layers, and no stacking variants are observed. In $SmGaSb_2$ (a = 4.3087(5) Å, c = 4.3319(4) Å) the difference between the cell parameters in the plane of the Ga chains is small, and in tetragonal $NdGaSb_2$ (a = b = 4.3486(3) Å) it is nonexistent. Once one layer of Ga chains has been placed over the $^2_\infty$[*RE*Sb_2] slab, there is little difference in energy between having the Ga chains in the next layer run parallel or perpendicular to those in the first. As discussed above, the $SmGaSb_2$ structure results if the Ga chains are always parallel, while in the $NdGaSb_2$ structure, the zigzag Ga chains alternate in direction. Why no intermediate stacking variants have been observed is not clear. Nor can we explain why certain rare-earth elements prefer either the $SmGaSb_2$ structure (La, Sm) or the $NdGaSb_2$ structure (Ce, Pr, Nd), crystallizing exclusively in one structure type.

Bonding. We can now attempt to apply the Zintl concept to *RE*$GaSb_2$. If we assume that the *RE* atoms, attaining a +3 oxidation state, participate in predominantly ionic bonds by donating their valence electrons to the anionic substructure, then we arrive at the formulation $RE^{3+}[(GaSb)(Sb)]^{3-}$. The assignment of oxidation states in the $^2_\infty$[GaSb] layer, which contains normal Ga−Sb and Ga−Ga single bonds, is straightforward. Since Sb is more electronegative than Ga, we first satisfy the Sb octets, neglecting any Ga−Sb bonding, and arrive at an oxidation state of −3 for the isolated Sb(1) atoms. Each Ga atom participates in two Ga−Ga bonds, and is therefore assigned an oxidation state of +1. On the basis of these oxidation state assignments, we can describe the layer as $^2_\infty[GaSb]^{2-}$, isoelectronic to the $^2_\infty[GeAs]^{1-}$ anionic substructure of the Zintl phase $BaGe_2As_2$ in which Ge, rather than Ga, chains occur.[17] To maintain charge balance, the remaining Sb atoms of the $^2_\infty$[Sb] square net must have an oxidation state of −1, consistent with each Sb atom participating in four half-bonds. The concept of intermediate one-electron Sb−Sb bonds has been used to successfully rationalize the bonding in a variety of compounds, and has now gained acceptance.[3−6,31]

To a first approximation, then, the Zintl concept leads to a bonding model for *RE*$GaSb_2$ in which the anionic substructure is composed of well-separated and noninteracting layers, $^2_\infty[GaSb]^{2-}$ and $^2_\infty[Sb]^{1-}$. To test the validity of this proposed

(30) (a) Pyykkö, P. *Chem. Rev.* **1997**, *97*, 597. (b) Mehrotra, P. K.; Hoffmann, R. *Inorg. Chem.* **1978**, *17*, 2187.

(31) Brylak, M.; Jeitschko, W. *Z. Naturforsch. B: Chem. Sci.* **1994**, *49*, 747.

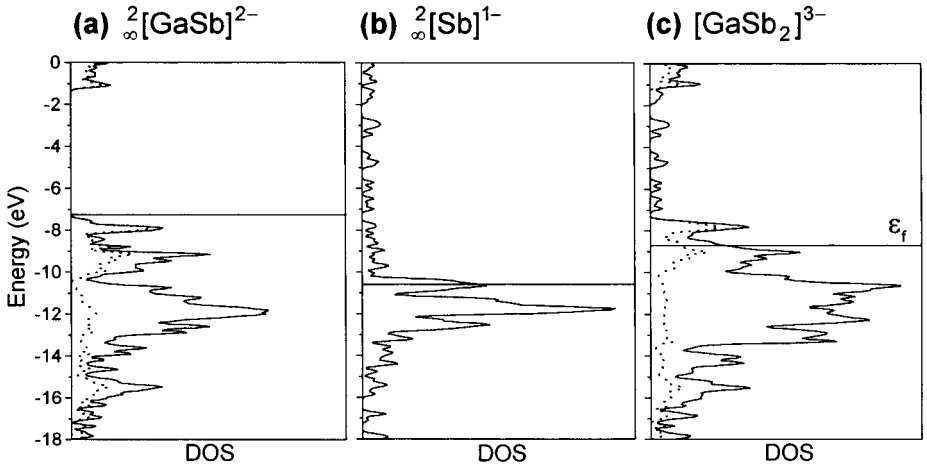

Figure 7. Density of states (DOS) for (a) the $^2_\infty[GaSb]^{2-}$ layer, (b) the $^2_\infty[Sb]^{1-}$ square net, and (c) the composite $[GaSb_2]^{3-}$ substructure of $SmGaSb_2$. The Ga projection is shown by the dotted line; what remains of the total DOS is the Sb projection. The Fermi level at −8.7 eV is shown by the horizontal line in part c.

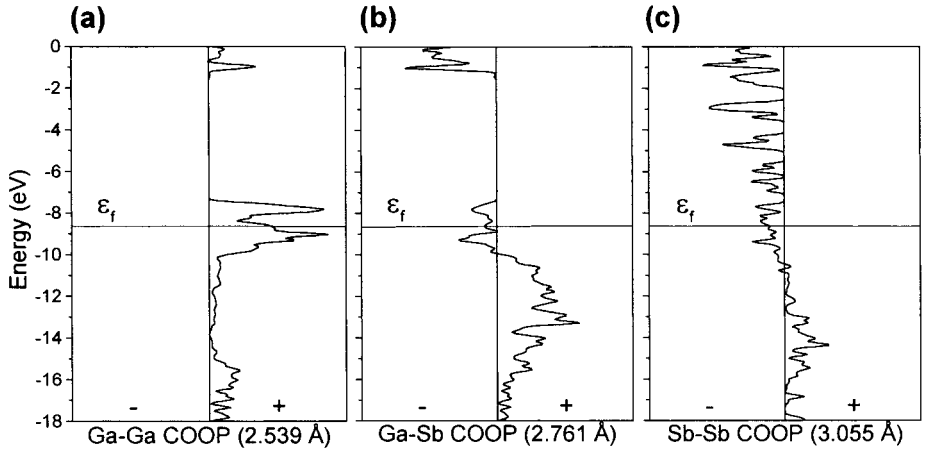

Figure 8. Crystal orbital overlap population (COOP) curves for (a) Ga−Ga (2.539(2) Å), (b) Ga−Sb (2.7606(12) Å), and (c) Sb−Sb (3.0549(2) Å) interactions in the $[GaSb_2]^{3-}$ substructure of $SmGaSb_2$.

bonding model, the band structure of the anionic $[GaSb_2]^{3-}$ substructure of the simpler $SmGaSb_2$ structure was calculated. As expected, the band structure of $[GaSb_2]^{3-}$ is simply a superposition of the band structures of each layer (Figure 7). In the density of states (DOS) curve for the $^2_\infty[GaSb]^{2-}$ layer (Figure 7a), the lower energy states originate largely from the more electronegative Sb, and the higher energy states, located just below a band gap near −7.5 eV, originate mainly from Ga. However, there is substantial mixing of the Ga and Sb states, indicative of the strong covalent character of the Ga−Sb bonding. If the octets of all atoms in the $^2_\infty[GaSb]^{2-}$ layer are completed, as required by the oxidation state assignment proposed above, then, at this electron count, all states up to the band gap are filled, in agreement with our description of this two-dimensional layer as a "Zintl layer". The DOS curve for the Sb square net (Figure 7b) shows a continuous distribution of energy levels, with no band gap between bonding and antibonding states. At the electron count required to produce a $^2_\infty[Sb]^{1-}$ layer, the Fermi level lies at −10.7 eV. However, when the $^2_\infty[GaSb]^{2-}$ and $^2_\infty[Sb]^{1-}$ layers are stacked to form the three-dimensional $[GaSb_2]^{3-}$ framework, the Sb square net acts as an electron sink, accepting electrons from the $^2_\infty[GaSb]$ layer into Sb−Sb antibonding levels. The position of the Fermi level is now equalized to −8.7 eV in the composite $[GaSb_2]^{3-}$ substructure (Figure 7c). The Fermi level falls in a region of moderate DOS, and metallic behavior is predicted for $SmGaSb_2$.

The nature of bonding in the $[GaSb_2]^{3-}$ framework can be clarified by closer inspection of the crystal orbital overlap population (COOP) curves for the Ga−Ga, Ga−Sb, and Sb−Sb interactions, shown in Figure 8. Even though the lowering of the Fermi level in the $^2_\infty[GaSb]$ layer weakens Ga−Ga bonding slightly (Figure 8a), the Ga−Sb bonding is strengthened slightly as antibonding levels are depopulated (Figure 8b). With these bonding levels largely filled, bonding within the $^2_\infty[GaSb]$ layer remains strong and covalent, as indicated by the Mulliken overlap populations determined for the Ga−Ga (0.58) and Ga−Sb (0.56) interactions. In the $^2_\infty[Sb]$ layer, the raising of the Fermi level causes some levels that are only weakly Sb−Sb antibonding to be occupied (Figure 8c). The overlap population for the Sb−Sb bonds is 0.35, approximately half of what is normally seen for full single bonds and consistent with bond length correlations.[32] The band structure thus validates the Zintl picture of these bonds as roughly half-bonds, and confirms the role of such Sb square nets as electron sinks by permitting some degree of electron acceptance which weakens the Sb−Sb bonds only slightly.[6,32]

When Ga is replaced by In, the substoichiometric point phase, $LaIn_{0.8}Sb_2$, in which the In zigzag chains of the $^2_\infty[In_{0.8}Sb]$ layer are randomly segmented by vacancies, results. The main differences between the $[GaSb_2]^{3-}$ and the $[In_{0.8}Sb_2]^{3-}$ band

(32) Papoian, G.; Hoffmann, R. *J. Solid State Chem.* **1998**, *139*, 8.

structures occur in the $^2_\infty[M\text{Sb}]$ layer contributions.[33] The energy states with a significant contribution from the less electronegative In are, in general, higher in energy than the corresponding Ga states, while the $^2_\infty[\text{Sb}]$ net contribution to the band structure is relatively unaffected by changes in the $^2_\infty[M\text{Sb}]$ layer. Accordingly, the Fermi level is at a higher energy in $[In_{0.8}Sb_2]^{3-}$ (−6.8 eV) than in $[GaSb_2]^{3-}$ (−8.7 eV). Even at a substoichiometric In site occupation, more Sb−Sb antibonding levels are filled in $[In_{0.8}Sb_2]^{3-}$ than in $[GaSb_2]^{3-}$. Assuming a rigid band model, addition of any electrons to $[In_{0.8}Sb_2]^{3-}$ to give a stoichiometric $[InSb_2]^{3-}$ structure would cause a dramatic weakening of the Sb−Sb bonding, but only a slight increase in In−In bonding. Vacancies are thus an inherent feature needed to stabilize the $[In_{0.8}Sb_2]^{3-}$ structure.[5] In contrast, in $[GaSb_2]^{3-}$, full occupation of the Ga sites maximizes the Ga−Ga bond strength, and the simultaneous weakening of the Sb−Sb bonding in the square net is less important.

The presence of unoccupied Ga−Ga bonding levels just above the Fermi level of $[GaSb_2]^{3-}$ suggests that at least partial substitution of Ga with an element having more valence electrons should be possible. When Ga is replaced by the obvious candidate, Ge, new ternary compounds, $RE_6Ge_{5-x}Sb_{11+x}$, with a different structure type are formed.[34] However, doping Sn for Ga is possible (which is not surprising, since the structures of $SmGaSb_2$ and $LaSn_{0.75}Sb_2$ are so similar). Preliminary experiments indicate the existence of a solid solution $LaGa_{1-x}Sn_xSb_2$ in a range that extends to at least $x \approx 0.6$. A single-crystal structure determined for one member, $LaGa_{0.9}Sn_{0.1}Sb_2$, shows that small amounts of Sn can be substituted for Ga without any distortion of the $SmGaSb_2$-type structure.[35] Further study of this system could provide some insight into the driving force responsible for the distortion from zigzag Ga to linear Sn chains, and the reason for substoichiometric occupation of the Sn site in $LaSn_{0.75}Sb_2$.

In conclusion, the *RE*−Ga−Sb system is a rich one that augments a growing family of ternary rare-earth main-group-element antimonides characterized by extensive homoatomic bonding of the main-group elements. The structure of $RE\text{GaSb}_2$ shares many common features with $La_{13}Ga_8Sb_{21}$ and $RE_{12}Ga_4Sb_{23}$, such as the presence of strong Ga−Ga bonds and ribbons or square nets of more weakly bonded Sb atoms.[4] However, whereas the Zintl concept has been successful here in accounting for the electronic structure of $RE\text{GaSb}_2$, as confirmed by the band structure calculations, it has difficulties in rationalizing the structures of $La_{13}Ga_8Sb_{21}$ and $RE_{12}Ga_4Sb_{23}$. It is precisely in these regions of muddy applicability (intermediate electronegativity differences) where new or unusual modes of bonding are likely to be found; the challenge is for us to discover and understand them.

Acknowledgment. This work was supported by the Natural Sciences and Engineering Research Council of Canada and the University of Alberta. We thank Dr. Robert McDonald (Faculty Service Officer, X-ray Crystallography Laboratory) for the data collection and Ms. Christina Barker (Department of Chemical and Materials Engineering) for assistance with the EDX measurements.

Supporting Information Available: Listings of powder X-ray diffraction data for $RE\text{GaSb}_2$ (RE = La−Nd, Sm), further crystallographic details for $SmGaSb_2$ and $NdGaSb_2$ (PDF), and an X-ray crystallographic file in CIF format. This material is available free of charge via the Internet at http://pubs.acs.org.

JA003705+

(33) Mills, A. M.; Mar, A. Unpublished calculations.
(34) Lam, R.; McDonald, R.; Mar, A. *Inorg. Chem.* In press.
(35) Mills, A. M.; Mar, A. Unpublished results.